ETH Library

Dual configuration of shallow acceptor levels in 4H-SiC

Journal Article

Author(s):
Bathen, Marianne; Kumar, Piyush; Ghezellou, Misagh; Belanche Guadas, Manuel; Vines, Lasse; Ul-Hassan, Jawad; Grossner, Ulrike

Publication date:
2024-07

Permanent link:
https://doi.org/10.3929/ethz-b-000668680

Rights / license:
Creative Commons Attribution 4.0 International

Originally published in:
Materials Science in Semiconductor Processing 177, https://doi.org/10.1016/j.mssp.2024.108360

This page was generated automatically upon download from the ETH Zurich Research Collection.
For more information, please consult the Terms of use.

Materials Science in Semiconductor Processing 177 (2024) 108360

Contents lists available at ScienceDirect

Materials Science in Semiconductor Processing

journal homepage: www.elsevier.com/locate/mssp

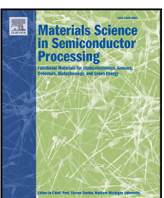

Full length article

Dual configuration of shallow acceptor levels in 4H-SiC

Marianne Etzelmüller Bathen [a,b,*], Piyush Kumar [a], Misagh Ghezellou [c], Manuel Belanche [a], Lasse Vines [b], Jawad Ul-Hassan [c], Ulrike Grossner [a]

[a] Advanced Power Semiconductor Laboratory, ETH Zürich, Physikstrasse 3, 8092 Zürich, Switzerland
[b] Department of Physics/Centre for Materials Science and Nanotechnology, University of Oslo, 0316 Oslo, Norway
[c] Department of Physics, Chemistry, and Biology (IFM), Linköping University, SE-581 83, Linköping, Sweden

ARTICLE INFO

Keywords:
Silicon carbide
Acceptor dopants
Electrically active defects
Minority carrier transient spectroscopy
Density functional theory

ABSTRACT

Acceptor dopants in 4H-SiC exhibit energy levels that are located deeper in the band gap than the thermal energy at room temperature (RT), resulting in incomplete ionization at RT. Therefore, a comprehensive understanding of the defect energetics and how the impurities are introduced into the material is imperative. Herein, we study impurity related defect levels in 4H-SiC epitaxial layers (epi-layers) grown by chemical vapor deposition (CVD) under various conditions using minority carrier transient spectroscopy (MCTS). We find two trap levels assigned to boron impurities, B and D, which are introduced to varying degrees depending on the growth conditions. A second acceptor level that was labeled X in the literature and attributed to impurity related defects is also observed. Importantly, both the B and X levels exhibit fine structure revealed by MCTS measurements. We attribute the fine structure to acceptor impurities at hexagonal and pseudo-cubic lattice sites in 4H-SiC, and tentatively assign the X peak to Al based on experimental findings and density functional theory calculations.

1. Introduction

Silicon carbide is rapidly becoming a popular choice for energy efficient power devices operating under harsh conditions [1]. However, defects that are introduced unintentionally during growth of 4H-SiC epitaxial layers (epi-layers) can have a debilitating impact on the device performance. For example, the carbon vacancy (V_C) is perennially present in state of the art 4H-SiC epi-layers to densities of $\sim 5 \times 10^{12}$ cm^{-3} [2] and post-growth treatments based on carbon injection [3–6] are needed for its removal. Notably, the V_C introduces two defect level signatures that can be detected by capacitance transient methods: the $Z_{1/2}$ assigned to the (0/2-) negative-U charge transition level of the V_C, and the $EH_{6/7}$ assigned to the V_C(2+/+/0) double donor transition [7]. The V_C related defect levels are commonly accepted as being responsible for reducing the minority carrier lifetime in 4H-SiC epi-layers [8,9] and substantial research has gone towards reducing the V_C density [3–6].

Recently, we demonstrated that impurity related defects can have a significant impact on material properties with the possibility of being detrimental to device performance. Indeed, n-type 4H-SiC samples with higher densities of boron impurity related acceptor levels compared to otherwise identical as-grown 4H-SiC epi-layers were found to exhibit a clear correlation with lower minority carrier lifetimes [10]. Two acceptor levels assigned to boron, the so-called B peak and D-center, are often observed in as-grown n-type 4H-SiC epi-layers using minority carrier transient spectroscopy (MCTS). The B peak is commonly accepted as originating from B on the Si lattice site (B_{Si}) and acts as a relatively shallow acceptor at $(0.23 - 0.28)$ eV above the valence band edge (E_V), while the D-center is located deeper in the band gap at E_V+$(0.58 - 0.63)$ eV [11] and was recently assigned to B on the C site, B_C [12]. In Ref. [10], the deep boron-related D-center was found to have a comparable influence on the carrier lifetime to that of the $Z_{1/2}$ level, which was previously considered the most prominent lifetime killer in 4H-SiC epi-layers. For this reason, a deeper understanding of acceptor impurity related defects in 4H-SiC epi-layers is needed.

Aluminum (Al) is typically used for p-type doping of SiC, both because of shallower dopant levels than boron acceptors, and due to the observed relation between boron and the minority carrier lifetime. However, the Al shallow acceptor level is still located relatively far away from the valence band edge (E_V) at around E_V+0.19 eV [13] as compared to, e.g., the nitrogen (N) shallow donor in 4H-SiC (at $57 - 105$ meV below the conduction band edge, E_C [14]), leading to incomplete ionization of acceptor dopants in 4H-SiC at room temperature (RT). Furthermore, reported energy levels and capture cross-sections for the Al shallow acceptor level vary greatly in the literature (see, e.g., Refs. [13,15–17]).

* Corresponding author at: Department of Physics/Centre for Materials Science and Nanotechnology, University of Oslo, 0316 Oslo, Norway.
E-mail address: m.e.bathen@fys.uio.no (M.E. Bathen).

https://doi.org/10.1016/j.mssp.2024.108360
Received 9 January 2024; Received in revised form 7 March 2024; Accepted 19 March 2024
Available online 1 April 2024
1369-8001/© 2024 The Authors. Published by Elsevier Ltd. This is an open access article under the CC BY license (http://creativecommons.org/licenses/by/4.0/).

Table 1
Sample details including identifier (ID), supplier, measured net doping density, and growth parameters for the studied epi-layers. The growth parameters include growth temperature (T), C/Si ratio, and whether doping was unintentional (U) or intentional (I) during growth. The net doping concentration was extracted from capacitance–voltage (CV) measurements of Schottky diodes.

ID	Supplier	Net doping (cm^{-3}) (μm)	T (°C)	C/Si	U/I
CR	CREE/Wolfspeed	1.05×10^{15}			I
C1	Linköping University	1.8×10^{14}	1640	1.2	I
D1	Linköping University	1.9×10^{14}	1600	1.05	U
F2	Linköping University	5.6×10^{13}	1640	1.1	U
L1	Linköping University	2.8×10^{13}	1640	1.3	I
E2	Linköping University	3.7×10^{13}	1640	1.1	U
G2	Linköping University	4.6×10^{12}	1640	1.1	U

Despite numerous studies on electrically active defects in 4H-SiC, many open questions remain, particularly related to the energetics and fine structure of acceptor impurities. Herein, we study as-grown n-type 4H-SiC epitaxial layers using MCTS measurements and illuminate the microscopic structure of shallow acceptor defect levels. Assignments to the sub-levels of shallow boron on Si site caused by the inequivalent hexagonal (*h*) and pseudo-cubic (*k*) lattice sites in 4H-SiC are provided. Furthermore, a second and shallower acceptor level, labeled X in the literature [18], is studied and tentatively assigned to Al impurities substituting on the Si lattice site based on experimental findings and density functional theory (DFT) calculations.

2. Methods

2.1. Experiment

We compare as-grown 4H-SiC epitaxial layers grown under varying conditions in different reactors and having a broad spread in net carrier concentration and growth conditions. The epi-layers were either purchased from CREE/Wolfspeed or grown by chemical vapor deposition (CVD) in a horizontal hot-wall reactor at Linköping University. All the epi-layers studied herein have (0001) orientation and a 4° off-cut towards the [11$\bar{2}$0] direction. The sample details are summarized in Table 1.

The wafers purchased from CREE/Wolfspeed have 10 μm thick epi-layers with net n-type doping (nitrogen) of $\sim 1.05 \times 10^{15}$ cm^{-3} as determined by capacitance–voltage (CV) measurements, and are grown on highly doped n^+ substrates with $\sim 8 \times 10^{18}$ cm^{-3} carrier density. Additionally, n-type 4H-SiC epi-layers were grown in a horizontal hot-wall CVD reactor at Linköping University with 20–25 μm thickness. Similar substrates as for the commercial samples were employed (highly doped and with $\sim 8 \times 10^{18}$ cm^{-3} carrier concentration). The non-commercial epi-layers were grown under different conditions including varying temperature, C/Si ratio, and intentional N doping while the rest of the growth conditions were kept constant. The growth rate was set to 25 μm h^{-1} for all non-commercial samples, where the change in C/Si ratio is provided by adjusting only the methane flow rates. The Si and C sources were trichlorosilane (TCS) and methane highly diluted in H_2, respectively. Molecular nitrogen gas (N_2) was used for intentional doping (I) while unintentionally doped (U) samples were doped by residual background nitrogen. Some of the samples used herein were also studied in Ref. [10].

To study electrically active defects that are present after epi-layer growth, Schottky diodes were formed using electron beam deposition of nickel (Ni) through a shadow mask. Metal deposition followed sample cleaning using a standard RCA procedure including a 2 min HF dip to remove the native oxide on the SiC surface. To facilitate probing of minority carriers, above band gap light must reach the space charge region of the Schottky diode to enable generation of electron–hole pairs. Thus, semi-transparent Schottky contacts were fabricated in a two-layer structure consisting of a lower layer of 600 μm or 900 μm diameter and ~10 nm thickness, and a top layer having 300 μm diameter and 100 nm thickness. The backside Ohmic contact was formed using silver paste. The net doping densities (N_D-N_A) were estimated by CV measurements of the Schottky contacts.

Defect levels in the semiconductor band gap can be studied using deep level transient spectroscopy (DLTS) for majority carrier traps and minority carrier transient spectroscopy (MCTS) for minority carrier traps. In this work, MCTS measurements were carried out to study acceptor impurity related defect levels in n-type 4H-SiC. The measurements were conducted at reverse biases (V_r) between −10 V and −1 V and in a temperature range of 20 K–350 K. The optical injection was induced by a 200 mW and 365 nm light emitting diode (LED) at a 100 ms or 200 ms pulse width (t_p) and with a period width (T_w) of 200 ms or 500 ms. The data shown herein represents the parameter set with the highest signal to noise ratio for each sample. Note that the reverse biases used for MCTS measurements herein are too small to probe the substrate considering the low doping densities in the epi-layers (see Table 1). Furthermore, all possible defects in the epi-layers are introduced during growth and therefore likely near-uniformly distributed in depth, meaning that the impact of using different reverse biases for MCTS measurements should be negligible.

The MCTS signal was extracted from the averaged transient over ~10 measurements at each temperature. A Fourier transform of the recorded transients was performed using up to 28 correlation functions. The spectrum referred to as the MCTS signal shown in the rest of the paper refers to the coefficient of the sine term (b_1) in the Fourier series of the deep level/minority carrier transient Fourier spectroscopy (DLTFS/MCTFS) [19]. Whenever other coefficients of the Fourier series besides b_1 are employed herein this will be explicitly specified.

Extraction of trap densities using DLTS follows (assuming the depletion approximation is valid)

$$N_t \approx 2\left(\frac{\Delta C}{C}\right)^{\max} N_{\mathrm{eff}}, \tag{1}$$

where $(\Delta C/C)^{\max}$ is obtained from the value of the signal at the peak maximum in the DLTS spectrum, N_t is the trap density and N_{eff} the doping concentration. Note that when estimating the concentration of a minority carrier trap using MCTS, N_t will depend on the free hole density that is induced by the applied optical pulse. Herein, we will use the net doping density $N_{\mathrm{eff}} = N_D - N_A$ measured by CV to estimate approximate hole trap concentrations [20], but note that these estimates will include inaccuracies as we do not know the exact induced hole concentration during light pulses.

Using Arrhenius analysis, the defect energy level (E_A) in the band gap and the apparent electron or hole capture cross-section ($\sigma_{n/p,\mathrm{app}}$) can be extracted from the MCTS spectra. It should be noted that the estimate for $\sigma_{n/p,\mathrm{app}}$ relies on the free carrier concentration. Herein, the net free electron concentration is used to estimate $\sigma_{p,\mathrm{app}}$ for the hole traps. The reason is that the induced hole concentration caused by the optical pulse during MCTS relies on multiple parameters including power and wavelength of the LED, transparency of the Schottky contact metal, and the diffusion of generated holes into the space charge region of the Schottky diode, and is challenging to determine. This contributes uncertainty to the estimated apparent capture cross-sections herein. Furthermore, the apparent capture cross-section can deviate from the measured one, $\sigma_{n/p,\mathrm{meas}}$, and contain contributions from additional

Table 2
Calculated chemical potential values using the HSE06 functional in the Si-poor/C-rich limit for the species studied herein (Si, C, N, Al).

Species	Unit cell	Chemical potential (eV)
Si	Si and SiC	−6.92
C	Diamond	−10.55
N	Si_3N_4 and Si	−12.43
Al	Al_4C_3 and diamond	−4.47

barriers for carrier capture. Since the induced hole concentration is unknown, we do not provide an estimate for $\sigma_{n/p,meas}$ herein, but instead report on $\sigma_{n/p,app}$ to compare between different defect levels.

To determine whether the defect concentration varies across the sample depth, the so-called depth profile (defect concentration as a function of depth from the surface) can be obtained by measuring the MCTS signal versus voltage at the maximum defect peak temperature. The depth profile is then calculated according to [21]

$$N_t(x) = -\left(\frac{qW^2 N_{eff}}{\epsilon_s \epsilon_0}\right) N_{eff}(x) \frac{\partial(\Delta C/C)}{\partial V}, \tag{2}$$

where W denotes the depletion region width, ϵ_s is the semiconductor permittivity, $N_{eff}(x)$ is the effective doping concentration depending on depth as obtained from CV measurements, and $\partial(\Delta C/C)/\partial V$ refers to the derivative of the MCTS signal with respect to voltage. We employ the net electron concentration to estimate the approximate concentration as a function of depth of hole traps herein since the induced hole concentration caused by optical pulses during MCTS could not be estimated.

2.2. Theory

Density functional theory (DFT) calculations in the Kohn–Sham (KS) formalism were performed to study the energetics and formation probabilities of impurity related defects in 4H-SiC. All DFT calculations were performed as implemented in the *Vienna ab initio Simulation Package* or VASP code [22–24] using the projector augmented-wave (PAW) method [25] to describe core electrons and plane waves to describe valence electrons. Both the lattice parameters and material and defect energetics were obtained using first the Perdew–Bruke–Ernzerhof (PBE) functional [26] for initial results, followed by calculations with the hybrid Heyd–Scuseria–Ernzerhof HSE06 functional [27] for improved accuracy. The HSE06 calculations yielded a band gap of 3.17 eV, in good agreement with the experimental value of 3.23 eV at RT [28]. Similarly, the computed lattice parameters of a = 3.070 Å and b = 10.048 Å agree with the experimental values (3.073 Å and 10.053 Å, respectively [29]).

For the defect calculations, 576-atom supercells were constructed by replicating the unit cell by 6 × 6 × 2 along the main axes. Defects were introduced in the supercell by removing a C or Si atom to form vacancies, and replacing them by an Al or N (for reference) atom to form substitutional defects. Defect relaxation was performed using PBE followed by HSE06. The HSE06 relaxation was performed using Γ-only Brillouin zone (BZ) sampling and a 450 eV energy cutoff, and with convergence criteria of 1×10^{-6} eV and 0.02 eV Å^{-1} for the electronic self-consistent loop and geometric relaxation, respectively. Defect formation energy (E^f) diagrams were formed according to [30]

$$E^f(q) = E^{tot}_{def}(q) - E^{tot}_{sc} - \Sigma_i n_i \mu_i + q(E_V + E_F) + E^{FNV}, \tag{3}$$

where q represents the charge state, $E^{tot}_{def/sc}$ refers to the total energy of the supercells with and without defect, respectively, n_i is the number of atoms added ($n_i > 0$) or removed ($n_i < 0$) from the supercell to create the defect, and μ_i is the chemical potential for each of the species (Si, C, Al, N). E_V refers to the valence band maximum and E_F is the Fermi level position relative to E_V. The formation energy diagrams are shown herein for the Si poor/C rich limit. The chemical potentials for Si and C were determined from the total energy per atom of the unit cell of Si and diamond, respectively. For the impurity atoms, the chemical potentials μ_N and μ_{Al} were obtained from Si_3N_4 and Al_4C_3, respectively. Table 2 contains the calculated (using the HSE06 functional) chemical potential values for the relevant species (Si, C, N and Al). E^{FNV} is a correction term to account for charged defects, and finite-size corrections were performed herein according to the Freysoldt–Neugebauer–van de Walle (FNV) correction scheme [31–33]. See Appendix for the computed FNV correction values for the different charge states of the impurity-related defects studied herein (i.e., N_C, N_{Si}, Al_C and Al_{Si}).

It should be noted that shallow dopants typically introduce delocalized states in the semiconductor band gap that are challenging to contain in a finite size supercell, and DFT calculations of shallow state defect levels are therefore expected to involve inaccuracies. Thus, the calculations performed herein are not intended to provide accurate defect levels, but rather to compare the formation probabilities of impurities on C vs. Si sites and to gauge any possible differences in energy level between impurities located at hexagonal (h) and pseudo-cubic (k) lattice sites in 4H-SiC.

3. Results and discussion

Fig. 1(a) shows MCTS spectra collected in the temperature range of 50 K–350 K for the as-grown epi-layers (see Table 1 for sample details) and reveals signatures from three levels in the lower part of the band gap, labeled X, B and D. The X, B and D peaks have previously been assigned to energy levels at 0.17 eV [18], 0.27 eV and 0.59 eV [11] above the valence band edge (E_V), respectively. We measure similar energy levels at E_V + 0.18 eV for the X, E_V + 0.28 eV for the B, and E_V + 0.58 eV for the D peak herein. The B level originates from the (0/-) acceptor transition of substitutional B on Si site (B_{Si}) [11,34], while the D defect signature was recently established as belonging to the (0/-) transition of substitutional B on the C site [12]. The X peak was previously observed and assigned to an impurity [18]. Table 3 lists the defect parameters that were extracted by Arrhenius analysis from the MCTS spectra shown in Fig. 1(a) for sample CR.

In Fig. 1(b), the same MCTS spectra are shown, but scaled by the net carrier (electron) density in the samples according to Eq. (1). It is evident that the impurity densities vary substantially across the samples. Most notable is the drastic difference in ratio between the X and B levels across the different samples. Indeed, the X peak is far more prominent relative to the B peak in the commercial sample (CR) as compared to those grown at Linköping University, where the B peak density consistently exceeds that of the X peak.

The X peak, in keeping with the behavior of the B and D peaks, does not change in intensity with irradiation [18,35,36]. This indicates an impurity related origin. According to Fig. 1, incorporation of the X impurity seems to depend strongly on the reactor or growth parameters used for epi-layer growth. The measured energy level position of around 0.18 eV for the X peak, combined with its impurity nature, indicates that Al is a likely candidate. Moreover, we measure an apparent hole capture cross-section of $\sigma_{p,app}$ =1.4×10^{-14} cm^2 for the X impurity (see Table 3), which is comparable to the defect assigned to the Al shallow acceptor level (E_A = 0.19 eV, $\sigma_{p,app}$ =1.4×10^{-13} cm^2) in Ref. [13] by thermal admittance spectroscopy. Note that one reported capture cross-section for the Al shallow acceptor based on current-DLTS (I-DLTS) measurements is suggested to be far lower at ∼1×10^{-19} cm^2 [17]. Unfortunately, the extracted concentration of the X level in the as-grown epi-layers studied herein (1×10^{11} cm^{-3}–1×10^{12} cm^{-3}) is too low for correlation with impurity concentrations using, e.g., secondary ion mass spectrometry (SIMS).

B on the Si site can localize in two different configurations in 4H-SiC, $B_{Si}(h)$ and $B_{Si}(k)$, depending on whether the impurity is located at the hexagonal (h) or pseudo-cubic (k) lattice site. B_{Si} situated at

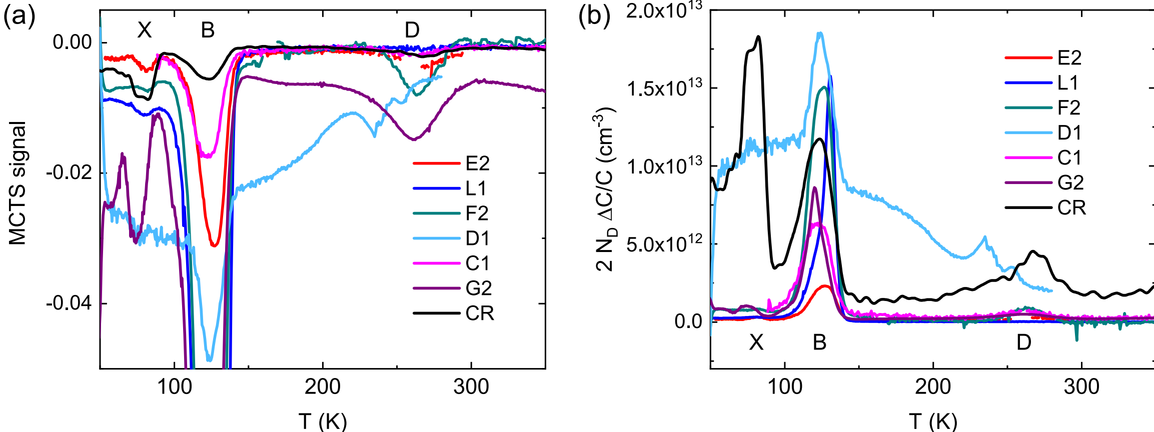

Fig. 1. (a) MCTS spectra collected in the 50 K–350 K temperature range at $V_r = -1$ V (samples CR, G2), $V_r = -3$ V (sample E2) and $V_r = -10$ V (samples F2, C1, D1, L1) reverse bias. Panel (b) shows the same data scaled by each sample's measured free carrier (electron) concentration at room temperature, i.e., $2N_{eff}\Delta C/C$.

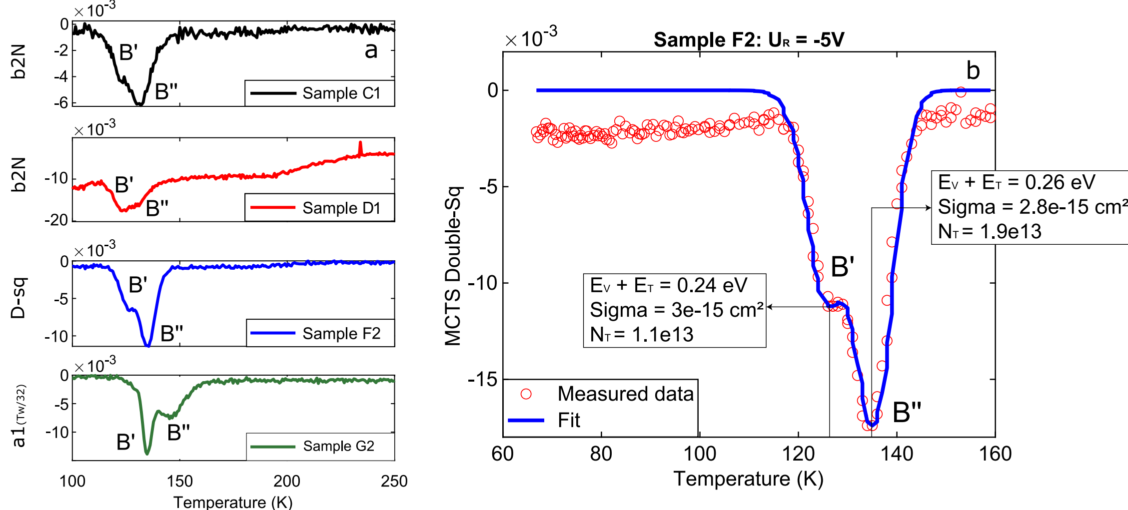

Fig. 2. (a) MCTS spectra in the 100 K–250 K temperature range that use different correlation functions to demonstrate the presence of two contributions to the shallow B peak in the C1, D1, F2 and G2 samples. (b) Fit (blue solid line) to the MCTS data (red dots) for the shallow B peak in sample F2, using the double-squared correlation function, and providing the trap parameters for the two contributions from the fit.

Table 3
Defect level parameters extracted by Arrhenius analysis of MCTS data for the CR sample.

Peak	$E_C - E_A$ (eV)	$\sigma_{p,app}$ (cm^2)	N_t (cm^{-3})
X	0.18	1.4×10^{-14}	1.2×10^{12}
B	0.28	1.1×10^{-14}	8.3×10^{11}
D	0.58	4.3×10^{-15}	1.9×10^{11}

the two different lattice sites, h and k, is expected to exhibit similar electronic properties and thermal stabilities, but where the hexagonal configuration $B_{Si}(h)$ has a slightly lower formation energy and the acceptor transition levels differ by 20 meV, as predicted by DFT [12]. Previous studies have attempted to separate these dual contributions to the B peak using Laplace-DLTS, especially since the D-center was recently shown to contain two distinct signatures assigned to B_C at h and k lattice sites [37], however without success. Fig. 2(a) shows MCTS spectra focusing on the B peak for as-grown epi-layers C1, D1, F2 and G2 using different coefficients of the Fourier transform (b2N, D-sq, a_1) than the sine term b_1. The figure clearly shows that there are two contributions to the B peak that are far enough separated that Laplace-DLTS is not necessary. We label the lower-temperature contribution B' and the higher-temperature one B''. A similar observation was recently reported in Ref. [38] as well. These two configurations, B' and B'', likely arise from B_{Si} on different lattice site configurations in 4H-SiC.

Fig. 2(b) shows a zoom-in of the MCTS data for sample F2 where the dual configuration of B_{Si} is clearly visible. The dots represent experimental data while the solid line is a fit containing estimated activation energies and apparent capture cross-sections. Here, the extracted parameters are E_A = 0.24 eV, $\sigma_{p,app}$ $=3 \times 10^{-15}$ cm^2 for B', and E_A = 0.26 eV, $\sigma_{p,app}$ $=2.8 \times 10^{-15}$ cm^2 for B''. In Ref. [12], the acceptor levels of $B_{Si}(k)$ and $B_{Si}(h)$ predicted by DFT were positioned at $E_V + 0.34$ eV and $E_V + 0.32$ eV, respectively, in decent agreement with experimental data despite a discrepancy that is within the expected uncertainty of both the experimental and theoretical methods. It should be noted that computing the capture cross-section is challenging and measurements are often accompanied by uncertainties of up to an order of magnitude. Indeed, the apparent and measured $\sigma_{n/p}$ can differ even more. These observations can at least partially explain the difference between charge transition levels predicted by DFT and estimated by fits to MCTS data for B_{Si} (0.24 eV and 0.26 eV above E_V from the simulated MCTS data, 0.32 eV and 0.34 eV from DFT calculations). Increasing the hole capture cross-section of B_{Si} by one order of magnitude, e.g., from $\sim 1 \times 10^{-15}$ cm^2 (close to the value in Fig. 2) to 1×10^{-14} cm^2, increases the accompanying fitted trap level energies by 15 meV–20 meV for X', X'', B' and B''. Oppositely, a reduction in the capture cross-section from

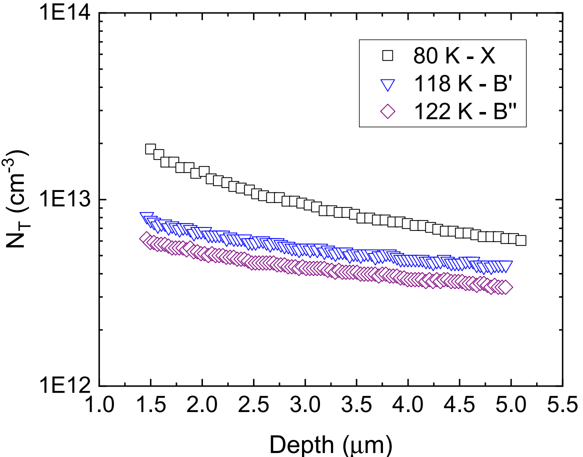

Fig. 3. MCTS depth profiles collected from sample CR at three different temperatures: 80 K centered at the X peak maximum, 118 K which coincides with the B' component of the B peak, and 122 K to probe the B" component.

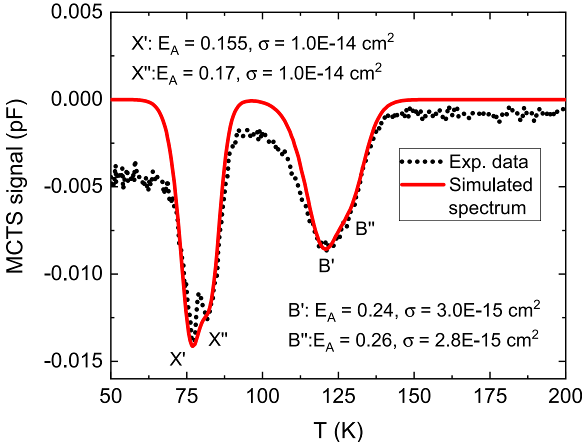

Fig. 4. Fitted (red) MCTS spectra (black) in the range 50 K–200 K demonstrating the presence of two contributions both to the X peak and the shallow B peak in sample CR. The total fit and its components are also illustrated in the figure. Measured data: T_w = 200 ms, t_p = 200 ms, V_r = −1 V.

1×10^{-15} cm^2 to 1×10^{-16} cm^2 reduces the acceptor trap level energies by 15 meV–20 meV. According to the fit to the MCTS curves, a hole capture cross-section as large as 1×10^{-12} cm^2 is needed for the trap levels of the B' and B" peaks to match those predicted for B_{Si} on *h* and *k* lattice sites by Ref. [12] using DFT calculations ($\sigma_p = 1 \times 10^{-12}$ cm^2 yields E_A of 0.31 eV and 0.33 eV above E_V for B' and B", respectively). Clearly, an accurate estimate of σ_p is essential for deducing the trap level energy from MCTS data. In conclusion, the B' and B" contributions to the B peak are assigned to boron situated on hexagonal and pseudo-cubic Si sites, respectively.

Interestingly, the relative intensities of the B' and B" configurations vary across the samples and hence likely depend on the growth parameters (see Fig. 2). For samples C1 and F2, the intensity of B" exceeds that of B', while samples D1 and G2 exhibit higher intensities for the B' than B" configuration. In these experiments, the growth temperature was kept constant (except for sample D1, see Table 1), the samples were unintentionally doped apart from C1 and L1, and all samples were grown with similar cooling rates. The pairwise configuration dependence (C1 and F2 have B">B', D1 and G2 have B'>B") cannot be directly related to these growth conditions, and does not seem to be correlated with the carrier concentration or approximate B peak concentration either. It is possible that the preference of B_{Si} to localize in a specific configuration (*h* or *k* lattice site) is related to minute differences in the growth conditions, for example the manner in which doping is introduced and the cooling rate after the high-temperature growth procedure. One alternative explanation for the variation in B'/B" ratio is local temperature variations across the wafer during epi-layer growth that contribute to the observed differences in fine structure of the MCTS spectra in Fig. 2.

Depth profiling of the two shallow acceptor levels, X and B, was performed to further elucidate their origin and incorporation mechanism, and determine their internal relations. Fig. 3 shows MCTS depth profiles collected from sample CR at three different temperatures: 80 K centered at the X peak maximum, 118 K which coincides with the B' component of the B peak, and 122 K to probe the B" configuration. Interestingly, the X and B defects are near-uniformly distributed in depth, but all depth profiles exhibit a slight increase towards the surface within the probed region. This indicates accumulation of acceptor-like impurities towards the surface of the epi-layers during growth. Further, the two components of the B peak, B' and B", exhibit the same profile variation across the probed region (see Fig. 3). This supports the assignment of B' and B" to hexagonal and pseudo-cubic components of shallow boron on the Si lattice site. The X peak, on the other hand, shows a steeper increase towards the epi-layer surface. This indicates an origin related to a different acceptor impurity than B, with Al being a prominent candidate considering the measured energy level and capture cross-section parameters (see Table 3). In fact, the increase in density of the X peak towards the epi-layer surface is in agreement with previous studies that found accumulation of Al near the SiC surface after implantation and activation annealing [39]. This supports a tentative assignment of the X peak to an Al impurity situated on the Si lattice site. It should be noted that the Al implanted samples in Ref. [39] are highly doped, in contrast to the low concentrations of acceptor impurities in the samples studied herein. If the X peak does indeed arise from Al on a Si lattice site, the findings presented in Fig. 3 demonstrate that Al accumulation towards the surface occurs regardless of Al concentration and across a broad doping range.

Fig. 4 displays high-resolution MCTS measurements on sample CR that demonstrate the dual configuration of both the X and B peaks. In keeping with the labeling for B, the lower-lying configuration of X is labeled X', while the higher energy contribution is labeled X". The red curve in Fig. 4 is a fit to the data (black) based on simulated MCTS data and assuming two contributions to both the X (X' and X") and B (B' and B") peaks. The same parameters as shown in Fig. 2(b) are employed for fitting the B' and B" configurations in Fig. 4. Using an apparent capture cross-section $\sigma_{p,app}$ for the X defect of 1×10^{-14} cm^2 according to Table 3, the two configurations X' and X" have energy levels at 0.155 eV and 0.17 eV above E_V, respectively. The energetic separation of 15 meV between the X' and X" configurations of the X peak is comparable to that found for the B peak (20 meV) using both MCTS and DFT calculations, and supports an assignment to substitutional impurities at *h* and *k* lattice sites in 4H-SiC.

Fig. 5 shows formation energy diagrams for vacancy and dopant related defects in 4H-SiC calculated using DFT with the HSE06 functional and a 576-atom supercell. The defect centers depicted include the carbon and silicon vacancies (V_C and V_{Si}, respectively), nitrogen on C (N_C) and Si (N_{Si}) lattice sites, and aluminum on C (Al_C) and Si (Al_{Si}) lattice sites. Intriguingly, the N and Al related defect levels exhibit similar but opposite trends: on one of the atomic sites, the impurity behaves as a shallow dopant, while on the other, it is a deep level defect. For the case of nitrogen, the C site is preferred by several eV, while aluminum clearly prefers the Si site by an even larger margin.

The (0/-) acceptor level of Al_{Si} is predicted by DFT to be found at roughly 0.19 eV above the valence band edge (see Fig. 5), in excellent agreement with the measured energy level of 0.18 eV for the X peak herein (see Table 3). According to theoretical modeling, the separation between the *h* and *k* configurations of Al_{Si} is so small in terms of both formation energy and transition level that it is not visible in

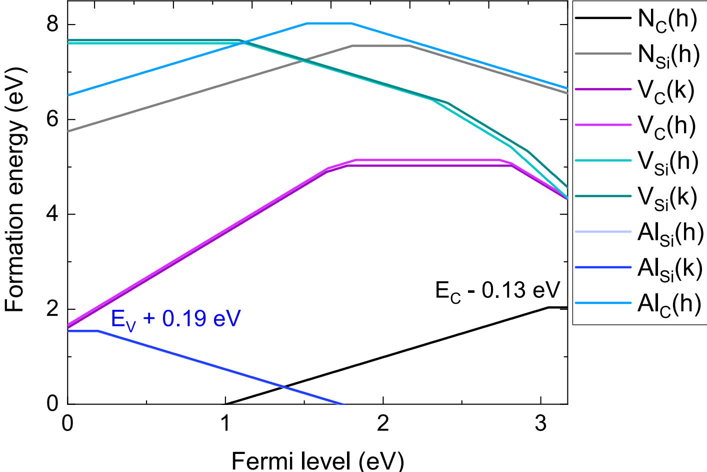

Fig. 5. Formation energy diagrams computed using DFT and the HSE06 functional in a 6 × 6 × 2 4H-SiC supercell. The data for V_C and V_{Si} was computed in Ref. [40].

Fig. 5. The predicted energetic separation between the two lattice sites is minute at only 4 meV, with $Al_{Si}(h)(0/-)$ landing at $E_V + 0.187$ eV, and $Al_{Si}(k)(0/-)$ located at $E_V + 0.191$ eV. This is far below the typical accuracy expected for this kind of calculation and also smaller than the separation between X' and X" (15 meV) extracted from the MCTS measurements (see Fig. 4). Nonetheless, we tentatively assign the X' and X" peaks to the *h* and *k* configurations, respectively, of Al on the Si site.

4. Concluding remarks

Controlled introduction of acceptor dopants is essential for the successful realization of SiC power devices. Herein, we study the presence of three impurity-related acceptor levels (X, B and D) that are introduced during growth of 4H-SiC epitaxial layers using minority carrier transient spectroscopy (MCTS). Firstly, epi-layers grown using different reactors and growth conditions exhibit different intensities of defect levels attributed to the B and X impurities. Both types of shallow acceptor impurities are found to accumulate towards the epi-layer surface by MCTS depth profiling but the trend is stronger for the X defect center. Furthermore, both the X and B peaks are found to exhibit a dual configuration — i.e., the X peak consists of the X' and X" contributions, while the two signatures labeled B' and B" are encompassed by the B peak. In the case of the B peak contributions, they are assigned to B_{Si} on the hexagonal (*h*) and pseudo-cubic (*k*) lattice sites for B' and B", respectively. A similar situation is expected for the X peak. Finally, the energy level position of the X peak, around ~0.19 eV above the valence band edge, combined with an extrinsic defect nature, suggests the Al impurity on Si site as a likely candidate for the defect origin.

CRediT authorship contribution statement

Marianne Etzelmüller Bathen: Conceptualization, Investigation, Formal analysis, Writing – original draft, Visualization, Validation, Project administration, Funding acquisition, Supervision. **Piyush Kumar:** Investigation, Formal analysis, Visualization, Writing – review & editing. **Misagh Ghezellou:** Investigation, Formal analysis, Writing – review & editing. **Manuel Belanche:** Investigation, Formal analysis, Writing – review & editing. **Lasse Vines:** Conceptualization, Resources, Writing – review & editing, Funding acquisition, Supervision. **Jawad Ul-Hassan:** Conceptualization, Resources, Writing – review & editing, Funding acquisition, Supervision. **Ulrike Grossner:** Conceptualization, Resources, Writing – review & editing, Funding acquisition, Supervision.

Declaration of competing interest

The authors declare that they have no known competing financial interests or personal relationships that could have appeared to influence the work reported in this paper.

Data availability

The data that support the findings of this study are available from the corresponding author upon reasonable request.

Acknowledgments

The work of MEB was supported by an ETH Zürich Postdoctoral Fellowship, Norway. Financial support was kindly provided by the Research Council of Norway and the University of Oslo, Norway through the frontier research project QuTe (no. 325573, FriPro ToppForsk-program) and the Norwegian Micro- and Nano-Fabrication Facility, NorFab, Norway, project number 295864. The financial support from the Swedish Energy Agency Energimyndigheten, Sweden Project Nos. 43611-1 and Swedish Research Council VR, Sweden Grant No. 2020-05444 is acknowledged. The computations were performed on resources provided by UNINETT Sigma2 — the National Infrastructure for High Performance Computing and Data Storage in Norway.

Appendix. Charge state corrections

Table A.1 lists the calculated values for the FNV corrections computed for the different charge states *q* of the impurity-related defects shown in Fig. 5 — i.e., N atoms on C and Si lattice sites, and Al dopants substituting for C and Si atoms. Note that only the hexagonal (*h*) lattice site of each defect is listed for brevity.

Table A.1
Calculated values of the FNV correction (meV) for the different charge states *q* of the impurity-related defects shown in Fig. 5 (N and Al substituting for C and Si atoms). Only the hexagonal (*h*) lattice site of each defect is listed for brevity. Empty slots indicate that a particular charge state was not found to be thermodynamically stable.

q	$N_C(h)$	$N_{Si}(h)$	$Al_{Si}(h)$	$Al_C(h)$
+1	74.7	111.2		124.7
0	0	0	0	0
−1		107.2	113.1	94.7

References

[1] T. Kimoto, J.A. Cooper, Fundamentals of Silicon Carbide Technology: Growth, Characterization, Devices and Applications, Wiley, 2014.

[2] B. Zippelius, J. Suda, T. Kimoto, High temperature annealing of n-type 4H-SiC: Impact on intrinsic defects and carrier lifetime, J. Appl. Phys. 111 (2012) 033515.

[3] L. Storasta, H. Tsuchida, T. Miyazawa, T. Ohshima, Enhanced annealing of the $Z_{1/2}$ defect in 4H-SiC epilayers, J. Appl. Phys. 103 (2008) 013705.

[4] T. Hiyoshi, T. Kimoto, Reduction of deep levels and improvement of carrier lifetime in n-type 4H-SiC by thermal oxidation, Appl. Phys. Express 2 (2009) 041101.

[5] T. Hiyoshi, T. Kimoto, Elimination of the major deep levels in n- and p-type 4H-SiC by two-step thermal treatment, Appl. Phys. Express 2 (2009) 091101.

[6] H.M. Ayedh, R. Nipoti, A. Hallén, B.G. Svensson, Elimination of carbon vacancies in 4H-SiC employing thermodynamic equilibrium conditions at moderate temperatures, Appl. Phys. Lett. 107 (2015) 252102.

[7] N.T. Son, X.T. Trinh, L.S. Løvlie, B.G. Svensson, K. Kawahara, J. Suda, T. Kimoto, T. Umeda, J. Isoya, T. Makino, T. Ohshima, E. Janzén, Negative-U system of carbon vacancy in 4H-SiC, Phys. Rev. Lett. 109 (2012) 187603.

[8] P.B. Klein, B.V. Shanabrook, S.W. Huh, A.Y. Polyakov, M. Skowronski, J.J. Sumakeris, M.J. O'Loughlin, Lifetime-limiting defects in n- 4H-SiC epilayers, Appl. Phys. Lett. 88 (2006) 052110.

[9] K. Danno, D. Nakamura, T. Kimoto, Investigation of carrier lifetime in 4H-SiC epilayers and lifetime control by electron irradiation, Appl. Phys. Lett. 90 (2007) 202109.

[10] M. Ghezellou, P. Kumar, M.E. Bathen, R. Karsthof, E.Ö. Sveinbjörnsson, U. Grossner, J.P. Bergman, L. Vines, J. Ul-Hassan, The role of boron related defects in limiting charge carrier lifetime in 4H–SiC epitaxial layers, APL Mater. 11 (2023) 031107.

[11] J. Zhang, L. Storasta, J.P. Bergman, N.T. Son, E. Janzén, Electrically active defects in n-type 4H–silicon carbide grown in a vertical hot-wall reactor, J. Appl. Phys. 93 (2003) 4708–4714.

[12] V.J.B. Torres, I. Capan, J. Coutinho, Theory of shallow and deep boron defects in 4H-SiC, Phys. Rev. B 106 (2022) 224112.

[13] K. Kawahara, H. Watanabe, N. Miura, S. Nakata, S. Yamakawa, Shallow and deep levels in Al^{+}-implanted p-type 4H-SiC measured by thermal admittance spectroscopy, in: Silicon Carbide and Related Materials 2014, in: Materials Science Forum, vol. 821, Trans Tech Publications Ltd, 2015, pp. 403–406.

[14] N. Assmann, C. Persson, A.Y. Kuznetsov, E.V. Monakhov, Fine structure in electronic transitions attributed to nitrogen donor in silicon carbide, Appl. Phys. Lett. 119 (2021) 262101.

[15] H. Matsuura, M. Komeda, S. Kagamihara, H. Iwata, R. Ishihara, T. Hatakeyama, T. Watanabe, K. Kojima, T. Shinohe, K. Arai, Dependence of acceptor levels and hole mobility on acceptor density and temperature in Al-doped p-type 4H-SiC epilayers, J. Appl. Phys. 96 (2004) 2708–2715.

[16] A. Koizumi, J. Suda, T. Kimoto, Temperature and doping dependencies of electrical properties in Al-doped 4H-SiC epitaxial layers, J. Appl. Phys. 106 (2009) 013716.

[17] M. Kato, J. Di, Y. Ohkouchi, T. Mizuno, M. Ichimura, K. Kojima, Hole capture cross section of the Al acceptor level in 4H-SiC, Mater. Today Commun. 31 (2022) 103648.

[18] N. Für, M. Belanche, C. Martinella, P. Kumar, M.E. Bathen, U. Grossner, Investigation of electrically active defects in SiC power diodes caused by heavy ion irradiation, IEEE Trans. Nucl. Sci. 70 (2023) 1892–1899.

[19] S. Weiss, R. Kassing, Deep level transient Fourier spectroscopy (DLTFS)—A technique for the analysis of deep level properties, Solid-State Electron. 31 (1988) 1733–1742.

[20] B. Hamilton, A.R. Peaker, D.R. Wight, Deep-state-controlled minority-carrier lifetime in n-type gallium phosphide, J. Appl. Phys. 50 (1979) 6373–6385.

[21] P. Blood, J.W. Orton, The Electrical Characterization of Semiconductors: Majority Carriers and Electron States, Academic Press Limited, London, 1992.

[22] G. Kresse, J. Hafner, Ab initio molecular dynamics for liquid metals, Phys. Rev. B 47 (1993) 558–561.

[23] G. Kresse, J. Hafner, Ab initio molecular-dynamics simulation of the liquid-metal–amorphous-semiconductor transition in germanium, Phys. Rev. B 49 (1994) 14251–14269.

[24] G. Kresse, J. Furthmüller, Efficiency of ab-initio total energy calculations for metals and semiconductors using a plane-wave basis set, Comput. Mater. Sci. 6 (1996a) 15–50.

[25] G. Kresse, J. Furthmüller, Efficient iterative schemes for Ab initio total-energy calculations using a plane-wave basis set, Phys. Rev. B 54 (1996b) 11169–11186.

[26] J.P. Perdew, K. Burke, M. Ernzerhof, Generalized gradient approximation made simple, Phys. Rev. Lett. 77 (1996) 3865–3868.

[27] J. Heyd, G.E. Scuseria, M. Ernzerhof, Hybrid functionals based on a screened Coulomb potential, J. Chem. Phys. 118 (2003) 8207–8215.

[28] P. Grivickas, V. Grivickas, J. Linnros, a. Galeckas, Fundamental band edge absorption in nominally undoped and doped 4H-SiC, J. Appl. Phys. 101 (2007) 123521.

[29] M. Levinshtein, S. Rumyantsev, M.S. Shur, Properties of Advanced Semiconductor Materials: GaN, AlN, InN, BN SiC, SiGe, 2001.

[30] C. Freysoldt, B. Grabowski, T. Hickel, J. Neugebauer, G. Kresse, A. Janotti, C.G. Van de Walle, First-principles calculations for point defects in solids, Rev. Modern Phys. 86 (2014) 253–305.

[31] C. Freysoldt, J. Neugebauer, C.G.V. de Walle, Fully Ab initio finite-size corrections for charged-defect supercell calculations, Phys. Rev. Lett. 102 (2009) 016402.

[32] Y. Kumagai, F. Oba, Electrostatics-based finite-size corrections for first-principles point defect calculations, Phys. Rev. B 89 (2014) 195205.

[33] T. Gake, Y. Kumagai, C. Freysoldt, F. Oba, Finite-size corrections for defect-involving vertical transitions in supercell calculations, Phys. Rev. B 101 (2020) 020102.

[34] T. Troffer, M. Schadt, T. Frank, H. Itoh, G. Pensl, J. Heindl, H.P. Strunk, M. Maier, Doping of SiC by implantation of boron and aluminum, Phys. Status Solidi a 162 (1997) 277–298.

[35] P. Kumar, M. Belanche, N. Für, L. Guzenko, J. Woerle, M.E. Bathen, U. Grossner, Energy-dependent impact of proton irradiation on 4H-SiC schottky diodes, Mater. Sci. Forum 1092 (2023) 187–192.

[36] M. Belanche, M.E. Bathen, P. Kumar, C. Dorfer, C. Martinella, U. Grossner, Minority carrier traps induced by neutron reactions with 4H-SiC, Defects Diffus. Forum 426 (2023) 23–28.

[37] I. Capan, T. Brodar, Majority and minority charge carrier traps in n-type 4H-SiC studied by junction spectroscopy techniques, Electron. Mater. 3 (2022) 115–123.

[38] T. Knezevic, E. JelaviĆ, Y. Yamazaki, T. Ohshima, T. Makino, I. Capan, Boron-related defects in n-type 4H-SiC schottky barrier diodes, Materials 16 (2023) 0, http://dx.doi.org/10.3390/Ma16093347.

[39] J. Müting, V. Bobal, T. Neset Sky, L. Vines, U. Grossner, Lateral straggling of implanted aluminum in 4H-SiC, Appl. Phys. Lett. 116 (2020) 012101.

[40] J. Woerle, M. Bathen, T. Prokscha, A. Galeckas, H. Ayedh, L. Vines, U. Grossner, Muon interaction with negative- U and high-spin-state defects: Differentiating between C and Si vacancies in 4 H - Si C, Phys. Rev. A 14 (2020) 054053.